Electronic Supplementary Information

Experimental Section

Materials: $Cu(NO_3)_2{\cdot}xH_2O$ (99.9%), S (99.9%), $CuCl_2{\cdot}2H_2O$ (99.0%), HCl (99.0%), CH_4N_2S, $(CH_2OH)_2$, thioacetamide, N-(1-naphthyl), sulfanilamide, para-(dimethylamino) benzaldehyde, salicylic acid, NaClO (5.5%), NaOH, $LiNO_3$, CH_3COCH_3, $C_6H_5Na_3O_7{\cdot}2H_2O$, Nafion (5.0% wt), $Na_2[Fe(CN)_5NO]{\cdot}2H_2O$, $N_2H_4{\cdot}H_2O$, NH_4Cl, H_2SO_4, HCl (99.0%), H_2O_2 (5.0%) and C_2H_5OH were obtained from Aladdin Ltd. (Shanghai, China). The ultrapure water was purified through a Millipore process. Ultra-pure Ar (99.999%) and N_2 (99.999%) were obtained from Chengdu Guoguang Chemical Co., Ltd. All reagents were analytical grade and did not further purify.

Preparation of CuS concave polyhedral superstructures (CuS-CPSs): 0.5 mmol $Cu(NO_3)_2{\cdot}xH_2O$ and 1 mmol sulfur powder were added into a 40 mL Teflon-lined stainless steel autoclave. Then add 32 mL of anhydrous ethanol and stir vigorously. The autoclave was kept at 180 °C for 12 h and then cooled naturally to the room temperature. Finally, the black precipitate was centrifuged and washed three times with deionized water and ethanol, then dried in vacuum at 60 °C.[1]

Preparation of CuS-CPSs/CP: Carbon paper (CP) was pretreated in 0.05 M H_2SO_4, and then was sequentially cleaned in ethanol and deionized water several times by sonication. 10 mg CuS-CPSs and 40 μL 5 wt% Nafion solution were dispersed in 960 μL ethanol/water ($V_{ethanol}/V_{water}$ = 3/1) followed by 20 min sonication to form a homogeneous ink. 10 μL ink was loaded onto a CP (1 × 1 cm^2) and dried under room temperature (CuS-CPSs loading: 0.1 mg cm^{-2}). The sample was obtained as CuS-CPSs/CP.

Preparation of CuS nanoparticles (CuS-NPs): 0.5 g of $Cu(NO_3)_2{\cdot}xH_2O$, 0.7 g of CH_4N_2S, and 20 mL of $(CH_2OH)_2$ were mixed in a beaker. The system was under initial vacuum and then nitrogen gas was introduced to minimize the exposure to air. The temperature was kept at 110 °C for ten minutes. A mixture of 5 mL of 1 M NaOH and 5 mL of $(CH_2OH)_2$ was injected into the beaker. The solution was then held for an additional five minutes before cooling down to room temperature. The CuS-NPs

were separated by centrifuging for 10 min at 10000 rpm. The CuS-NPs were washed five times with water quickly to remove the excessive ions and precursors.

Preparation of CuS nanosheet assemblies (CuS-NSAs): CuS-NSAs were prepared by a simple microwave-assisted heating method. First, 4 mmol $CuCl_2 \cdot 2H_2O$ and 5 mmol thioacetamide were mixed with deionized water (80 mL) and ethanol (40 mL) in a 250 mL beaker. Then, the mixture was stirred vigorously for 30 min at room temperature. Next, the synthetic reaction was carried out in a microwave reactor at 500 W for 10 min. After cooling to room temperature, large amounts of gray precipitates were obtained. Finally, the as-synthesized samples were separated by a centrifuge, washed five times with deionized water and ethanol, followed by vacuum drying for 12 h.

Characterizations: Power XRD data were acquired by a LabX XRD-6100 X-ray diffractometer with a Cu Kα radiation (40 kV, 30 mA) of wavelength 0.154 nm (SHIMADZU, Japan). The absorbance data of spectrophotometer was measured on SHIMADZU UV-1800 UV-vis spectrophotometer. SEM images were collected on a Gemini SEM 300 scanning electron microscope (ZEISS, Germany) at an accelerating voltage of 5 kV. TEM images were acquired on a HITACHI H-8100 electron microscopy (Hitachi, Tokyo, Japan) operated at 200 kV. XPS measurements were performed on an ESCALABMK II X-ray photoelectron spectrometer using Mg as the exciting source.

Electrochemical measurements: In this paper, we use an H-type electrolytic cell separated by a Nafion membrane which was protonated by boiling in ultrapure water, H_2O_2 (5%) aqueous solution and 0.5 M H_2SO_4 at 80 °C for another 2 h, respectively. A three-electrode configuration is used for electrochemical experiments using catalyst coated carbon paper as the working electrode, Ag/AgCl (filled with saturated KCl solution) as the reference electrode, and graphite rod as the counter electrode. The electrochemical experiments were carried out with an electrochemical workstation (CHI 660E) in N_2-saturated 0.1 M HCl solution. The potentials reported in this work were converted to reversible hydrogen electrode (RHE) scale via calibration with the following equation: $E_{RHE} = E_{Ag/AgCl} + 0.197\ V + 0.059 \times pH$ and the presented current density was normalized to the geometric surface area.

Determination of NH_3: Concentration of produced NH_3 was spectrophotometrically determined by the indophenol blue method.[2] 2 mL sample was removed from the cathodic chamber, then added into 1 mL of oxidizing solution containing NaClO (ρ_{Cl} = 4 ~ 4.9), then added 2 mL coloring solution containing 1 M NaOH solution, 5% $C_7H_6O_3$ and 5% $C_6H_5Na_3O_7 \cdot 2H_2O$, and 200 μL catalyst solution (0.1 g $Na_2[Fe(CN)_5NO] \cdot 2H_2O$ diluted to 10 ml with deionized water) in turn. Absorbance measurements were performed after one hour at λ= 655 nm. The concentration-absorbance curves were calibrated using standard NH_3 solution with a serious of concentrations. The standard curve (y = 0.385x + 0.048, R^2 = 0.999) shows good linear relation of absorbance value with NH_3 concentration by three times independent calibrations.

Determination of N_2H_4: N_2H_4 was estimated by the method of Watt and Chrisp.[3] The color reagent was a mixed solution of 5.99 g $C_9H_{11}NO$, 30 mL HCl and 300 mL C_2H_5OH. In detail, 5 mL electrolyte was removed from the electrochemical reaction vessel, and added into 5 mL prepared color reagent and stirred 15 min at 25 °C. The absorbance of such solution at the absorbance of 455 nm was measured to quantify the hydrazine yields with a standard curve of hydrazine (y = 0.469x + 0.0523, R^2 = 0.999).

Determination of NO_3^-: The content of the NO_3^- in electrolyte can be quantitatively determined by spectrophotometer measurement.[4] 0.10 mL of 1.0 M HCl were added into 5.0 mL of standard $LiNO_3$ solution. After standing for 5 min, the concentration of NO_3^- was measured using UV-vis spectrophotometer at wavelength range from 200 to 300 nm. The standard curve (y = 0.084x + 0.001, R^2 = 0.999) shows good linear relation of absorbance value with NO_3^- concentration by three times independent calibrations.

Determination of NO_2^-: Spectrophotometer measurement[4] was utilized to estimate the content of the NO_2^-. In detail, 0.10 mL of sulfanilamide solution (0.50 g of sulfanilamide was dissolved in 50.0 mL of 2.0 M HCl solution) was added into 5.0 mL of electrolyte, then adding 1 mg/mL N-(1-naphthyl) solution in turn. Stand for 30 min at room temperature. The UV–vis spectrophotometer at wavelength ranges from 450 to 650 nm. The absorbance of such solution at 545 nm was measured to quantify the NO_3^- concentration by a standard curve (y = 1.777x + 0.007, R^2 = 0.999).

Determination of FE and V_{NH3}: FE was calculated by equation:

$$FE = [3F \times c_{NH3} \times V / (17 \times Q)] \times 100\%$$

NH_3 yield (V_{NH3}) was calculated using the following equation:

$$V_{NH3} = (c_{NH3} \times V) / (t \times m)$$

The mass of NH_3 was calculated as follows:

$$m_{NH3} = c_{NH3} \times V$$

Where F is the Faraday constant (96500 C mol^{-1}); c_{NH3} is the measured NH_3 concentration; Q is the total quantity of applied electricity; V is the volume of the HCl electrolyte for NH_3 collection (35 mL); t is the electrolysis time (2 h) and m is the catalyst loading mass (0.1 mg).

Computational methods

The spin-polarized first-principles DFT calculations were performed using the Vienna Ab initio Simulation Package (VASP).[5-7] The Perdew-Burke-Ernzerhof (PBE) exchange-correlation functional[8] within the generalized gradient approximation (GGA) was employed to describe the exchange-correlation energy. The projector-augmented-wave (PAW) method[9] was adopted for the pseudopotentials. The energy cutoff for the plane wave basis expansion was set to 450 eV. The force on each atom was set as 0.02 eV/Å for convergence criterion. Slab model was constructed in a 1×4×1 supercell with three layers of CuS (103), where the bottom layer was fixed. A vacuum layer of 15 Å in the z direction avoids the interaction between layers. The Brillouin-zone integration was sampled by single Γ point.[10]

The free energies of the NRR steps were calculated using the equation:[11]

$$\Delta G = \Delta E_{DFT} + \Delta E_{ZPE} - T\Delta S$$

Where ΔE_{DFT} is the DFT calculated binding energy, the ΔE_{ZPE} and TΔS are the zero-point energy correction and the variation of entropy, respectively, which gotten from vibration calculations.[12]

The surface energy of CuS can be evaluated by σ, which is defined as:

$$\sigma = (E_{(sur)} - N \times E_{(bulk)}) \times \frac{1}{2A}$$

in which $E_{(sur)}$ and $E_{(bulk)}$ are the energies of all research surface and bulk CuS, respectively. N is the number of bulk structure. A represents the surface area of each surface.

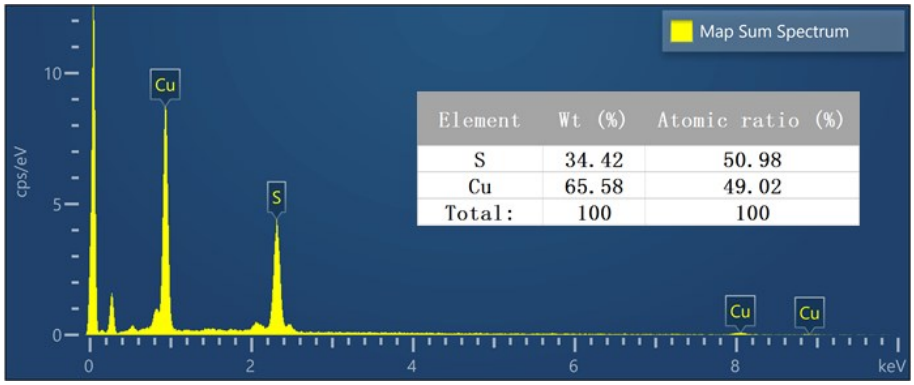

Fig. S1. EDX spectrum of CuS-CPSs.

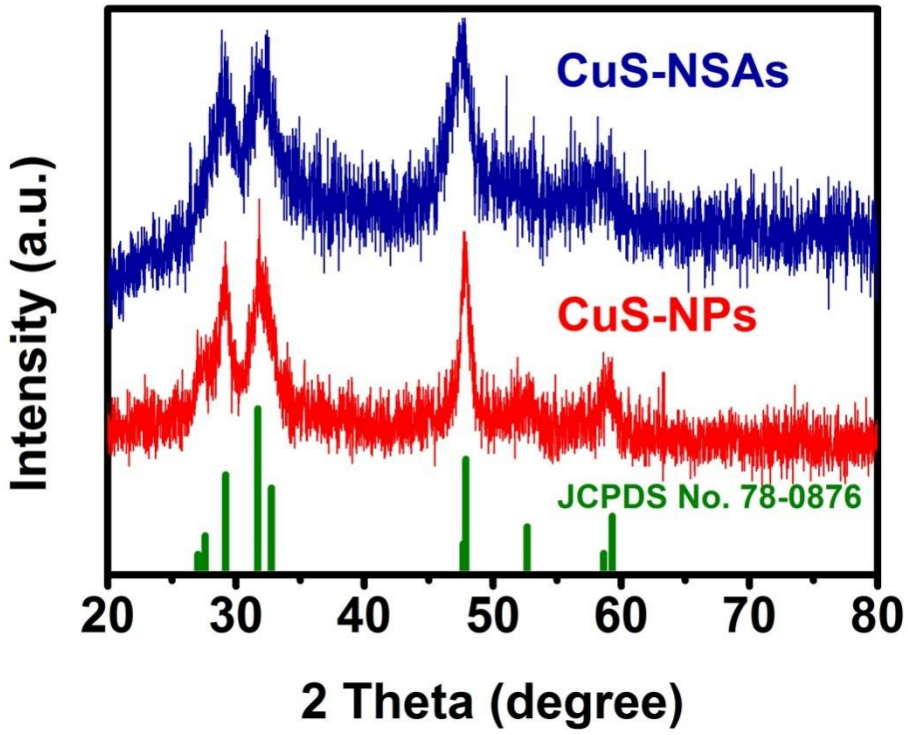

Fig. S2. XRD patterns of CuS-NPs and CuS-NSAs.

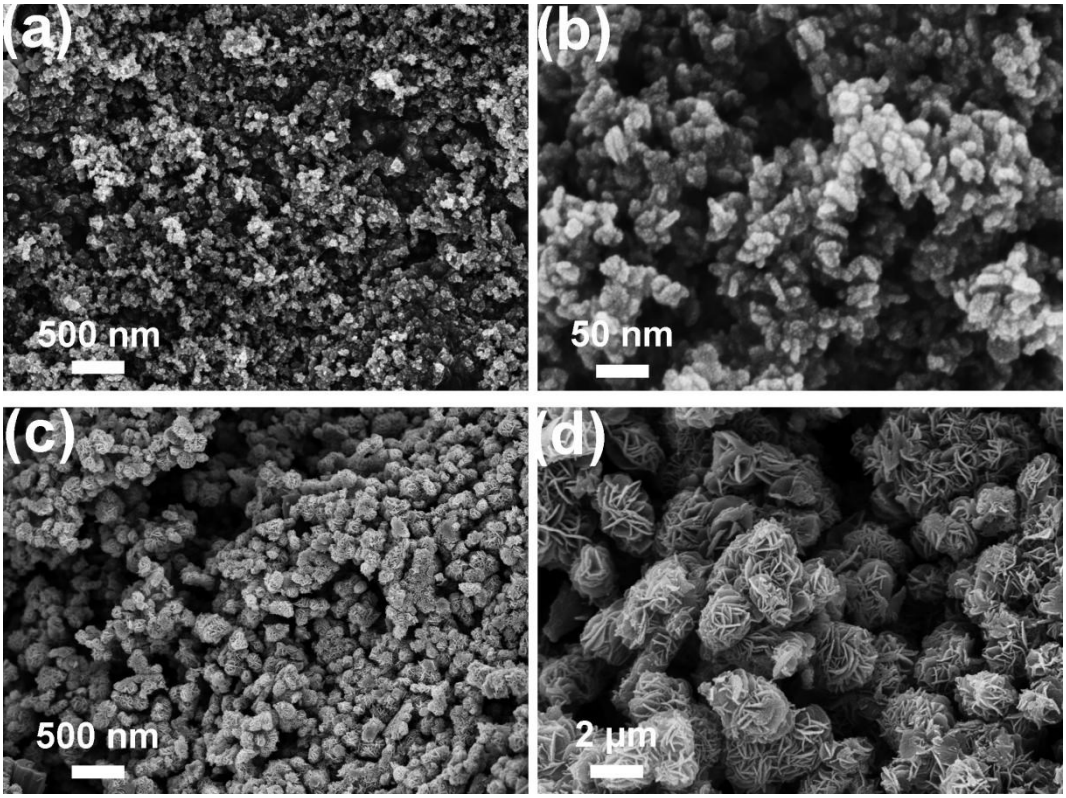

Fig. S3. SEM images of (a,b) CuS-NPs and (c,d) CuS-NSAs.

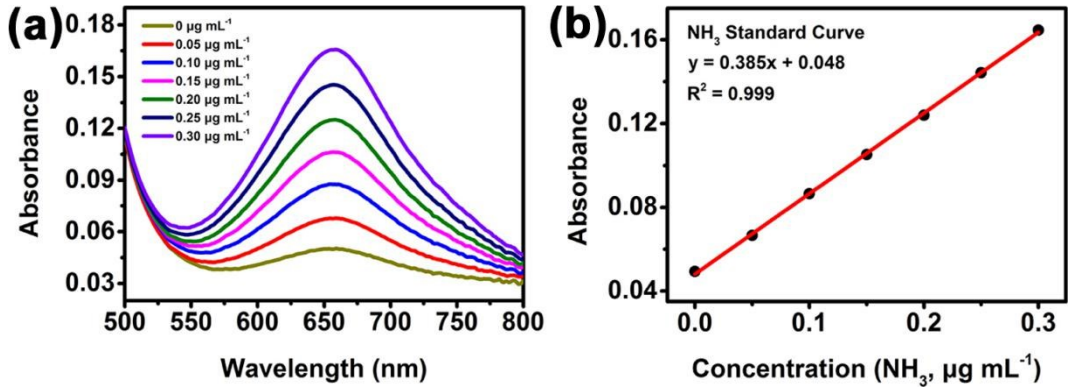

Fig. S4. (a) UV-vis absorption spectra of indophenol assays with NH_3 concentrations after incubated for 2 h at room temperature. (b) Calibration curve used for calculation of NH_3 concentrations.

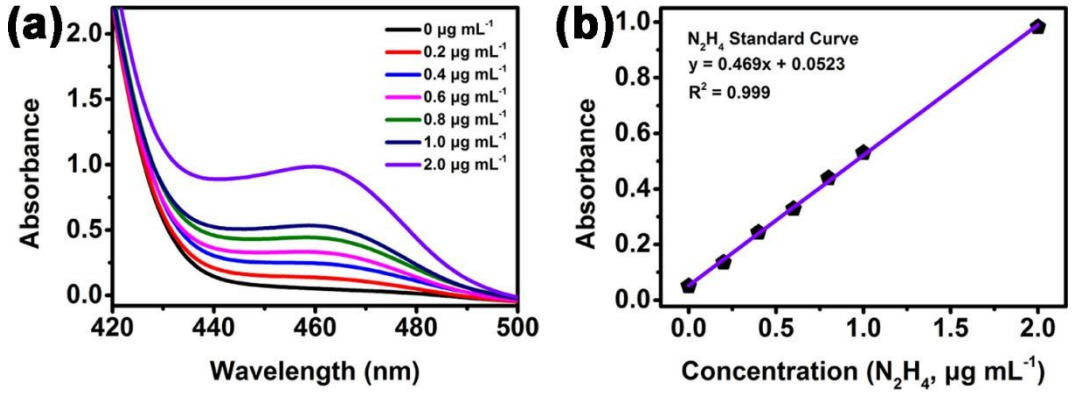

Fig. S5. (a) UV-vis absorption spectra of N_2H_4 concentrations after incubated for 20 min at room temperature. (b) Calibration curve used for calculation of N_2H_4 concentrations.

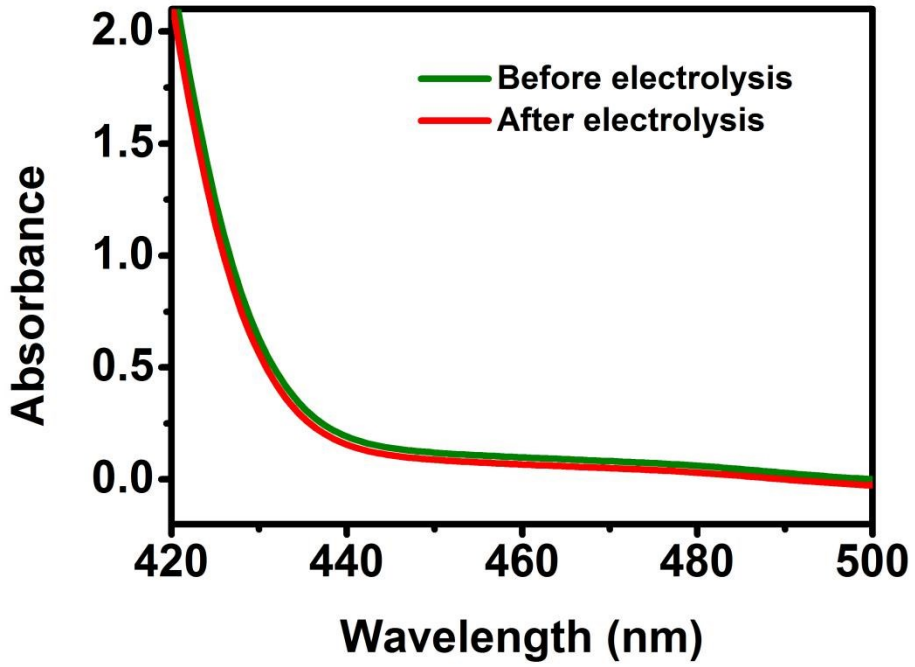

Fig. S6. UV-vis absorption spectra of electrolytes stained with para-(dimethylamino) benzaldehyde indicator before and after 2 h electrolysis at –0.15 V.

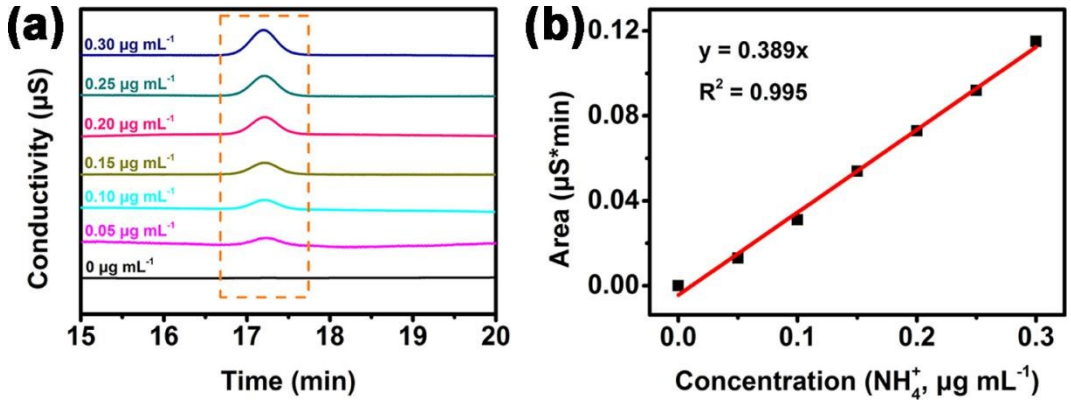

Fig. S7. (a) Ion chromatograms of NH_4^+ with different concentrations in 0.1 M HCl and (b) corresponding standard curve.

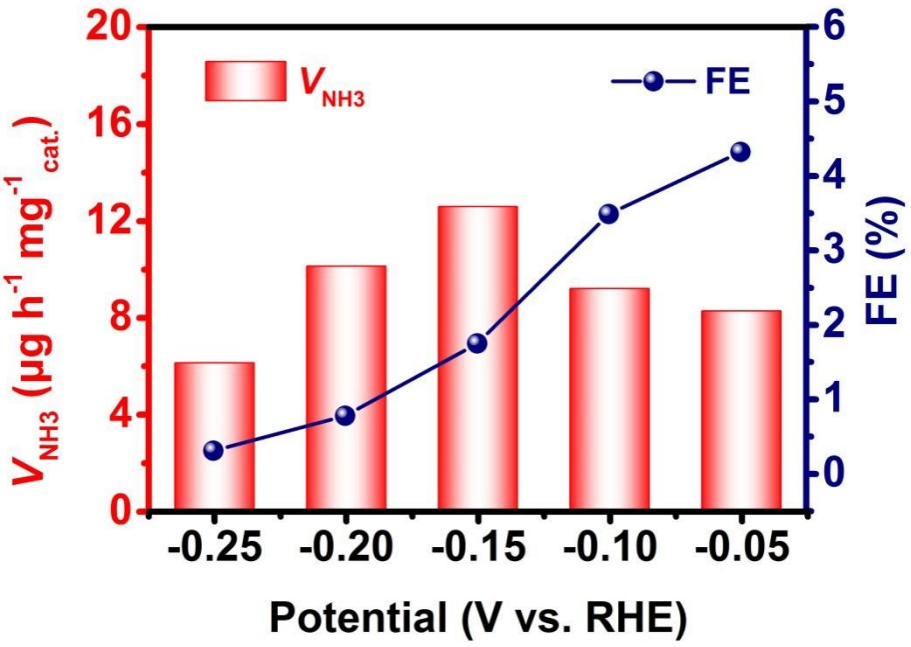

Fig. S8. V_{NH3} and FE for CuS-CPSs/CP tested in 0.1 M Na_2SO_4.

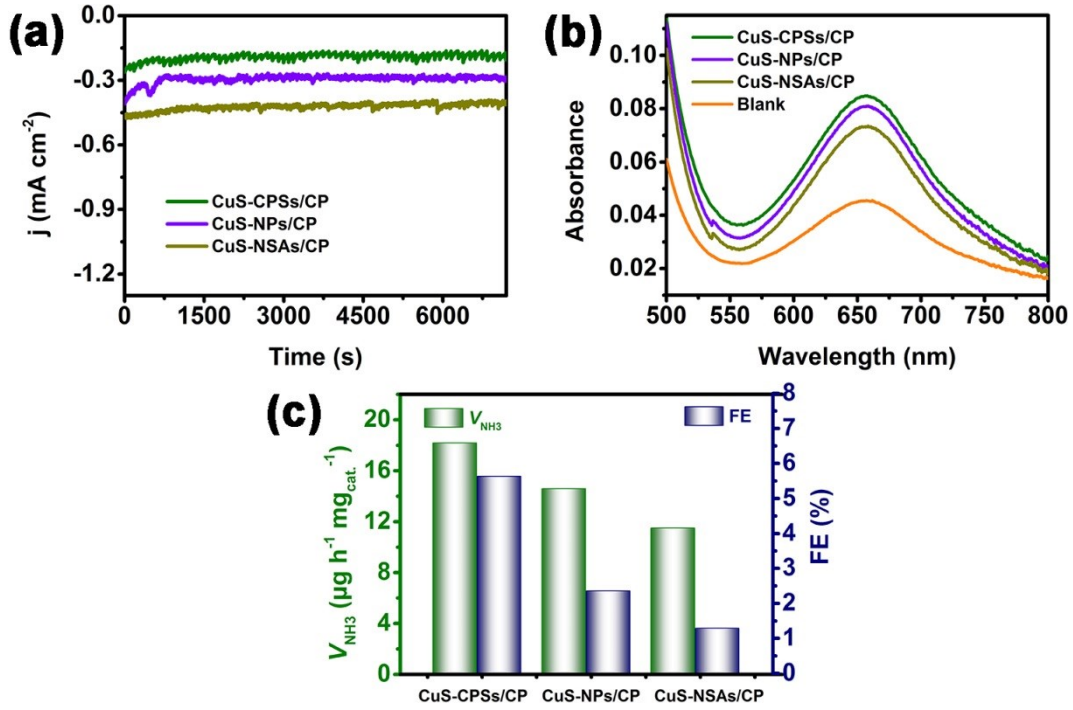

Fig. S9. (a) Time-dependent current density curves for CuS-CPSs/CP, CuS-NPs/CP and CuS-NSAs/CP at –0.15 V. (b) UV-vis absorption spectra of the electrolytes stained with indophenol indicator after 2 h electrolysis using CuS-CPSs/CP, CuS-NPs/CP and CuS-NSAs/CP. (c) Comparison of V_{NH3} and FE for CuS-CPSs/CP, CuS-NPs/CP and CuS-NSAs/CP.

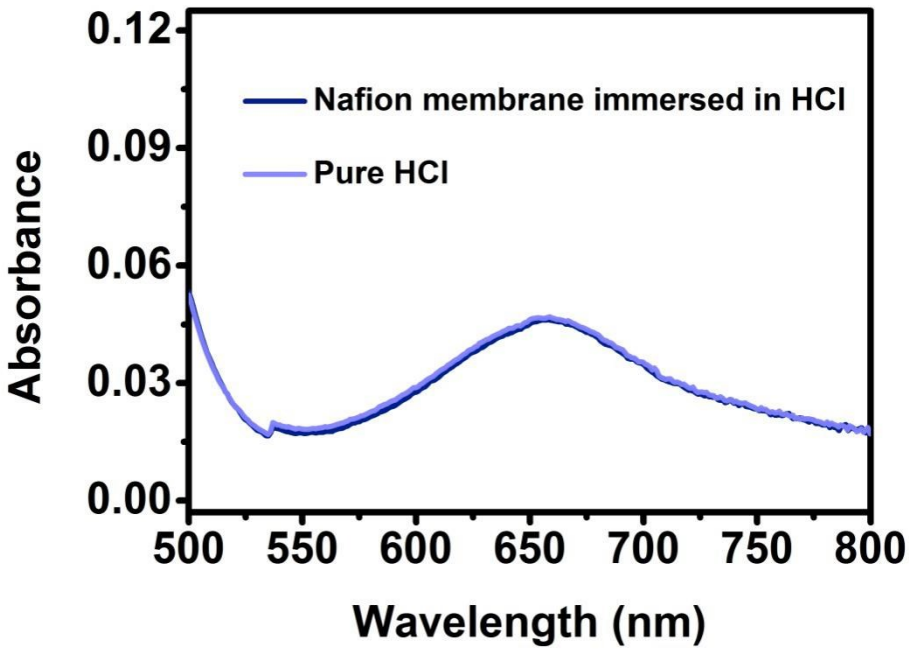

Fig. S10. Comparison of UV-vis absorption spectra of Nafion membrane immersed in 0.1 M HCl for 2 h and pure 0.1 M HCl.

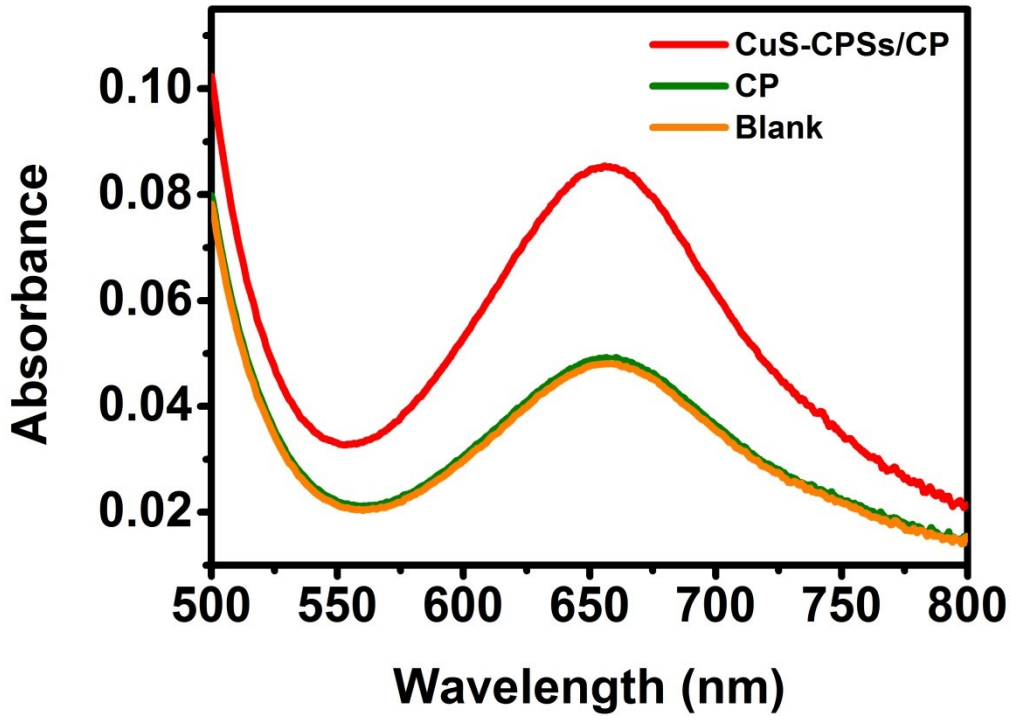

Fig. S11. UV-vis absorption spectra of the electrolytes colored with the indophenol indicator after NRR electrolysis at different electrodes for 2 h.

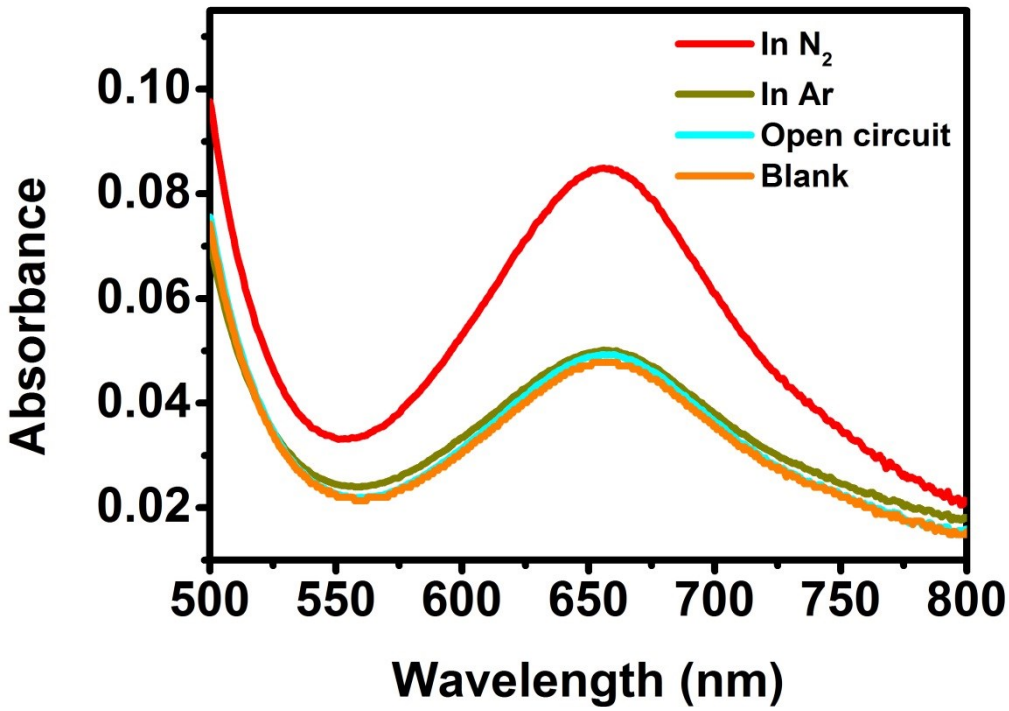

Fig. S12. UV-vis absorption spectra of the electrolytes stained with indophenol indicator after 2 h electrolysis under different electrochemical conditions using CuS-CPSs/CP.

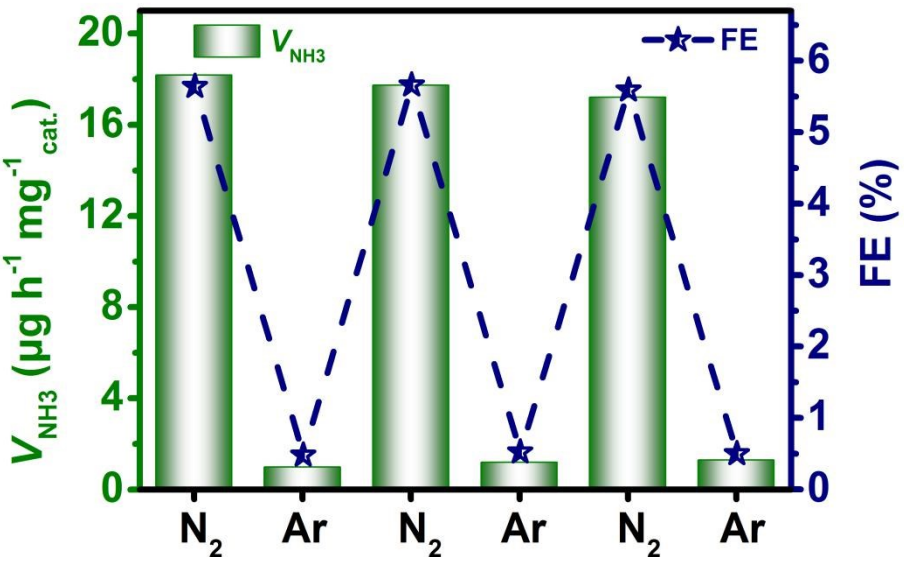

Fig. S13. V_{NH3} and FE of alternative N_2-saturated and Ar-saturated tests over CuS-CPSs/CP at –0.15 V for 2 h.

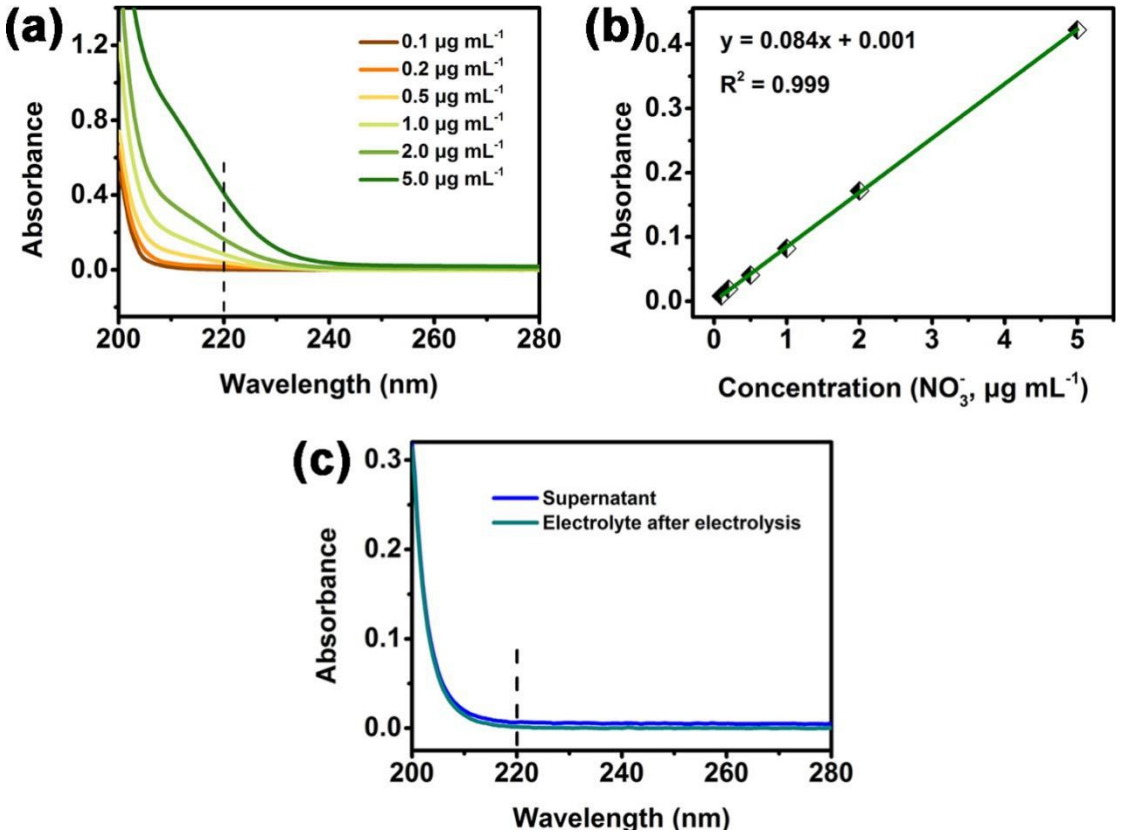

Fig. S14. (a) UV-vis absorption spectra of different concentrations of $LiNO_3$. (b) Calibration curve used for calculating the concentration of NO_3^-. (c) UV-vis absorption spectra for the determination of NO_3^- in the supernatant of the washed CuS-CPSs and in 0.1 M HCl after electrolysis.

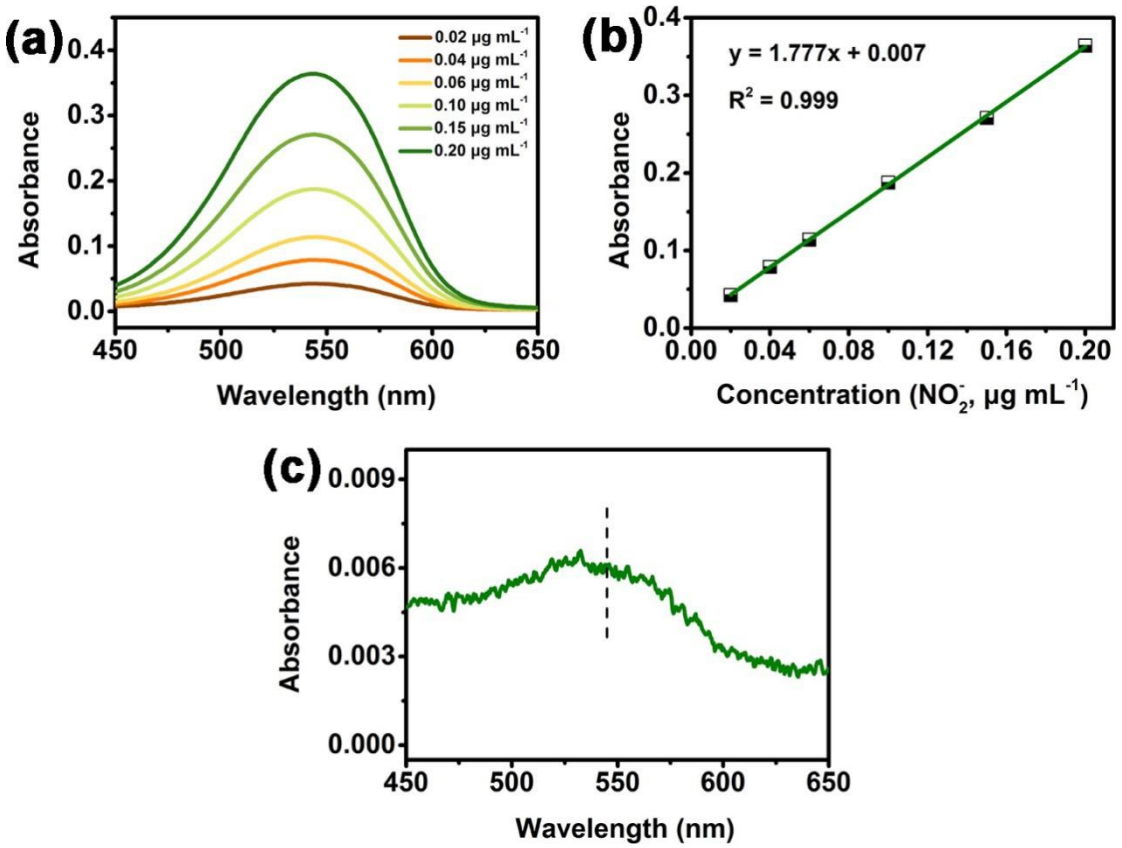

Fig. S15. (a) UV−vis spectra of various concentrations of $NaNO_2$. (b) Calibration curve used for calculating the concentration of NO_2^-. (c) UV−vis spectra for the determination of NO_2^- in 0.1 M HCl after electrolysis.

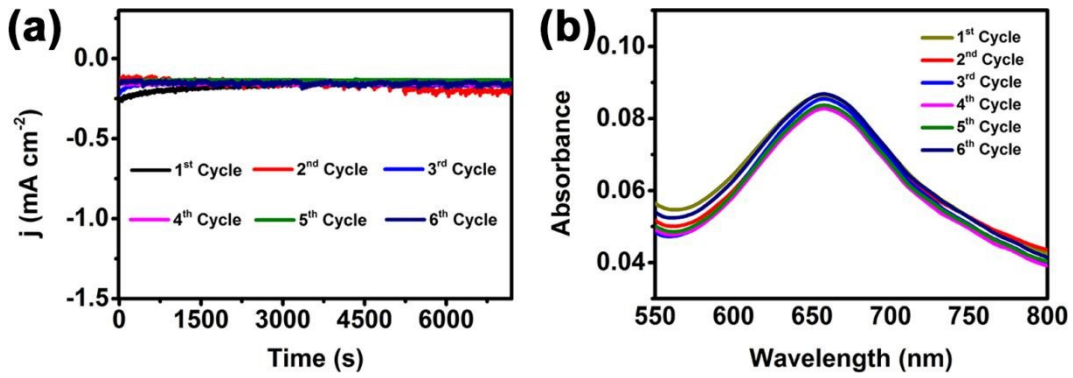

Fig. S16. (a) Time-dependent current density curves for CuS-CPSs/CP at –0.15 V over 6 cycles. (b) UV-vis absorption spectra of the electrolytes stained with indophenol indicator after electrolysis for CuS-CPSs/CP at –0.15 V over 6 cycles.

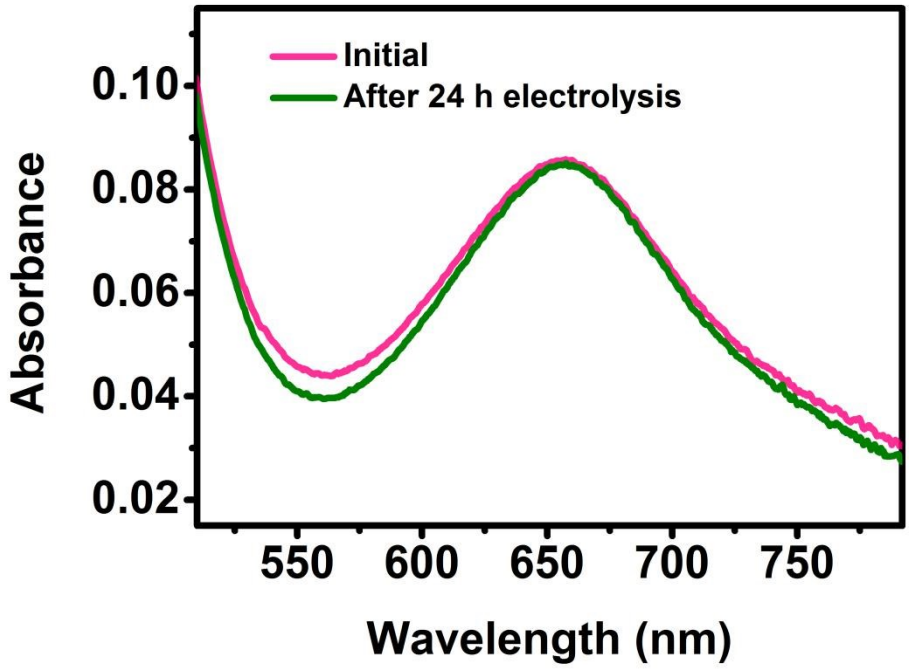

Fig. S17. UV-vis absorption spectra of the electrolytes stained with indophenol indicator at –0.15 V after electrolysis for 2 h with the initial CuS-CPSs/CP and the CuS-CPSs/CP after 24 h electrolysis.

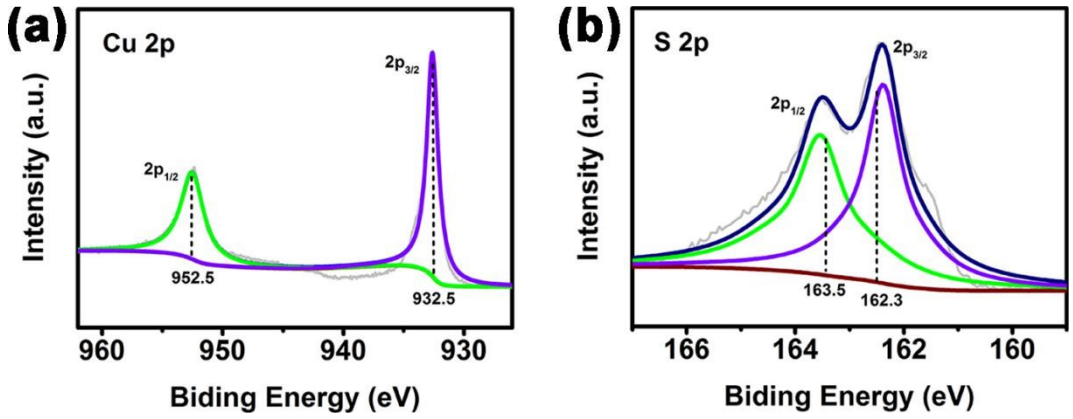

Fig. S18. XPS spectra of post-NRR CuS-CPSs in the (a) Cu 2p and (b) S 2p regions.

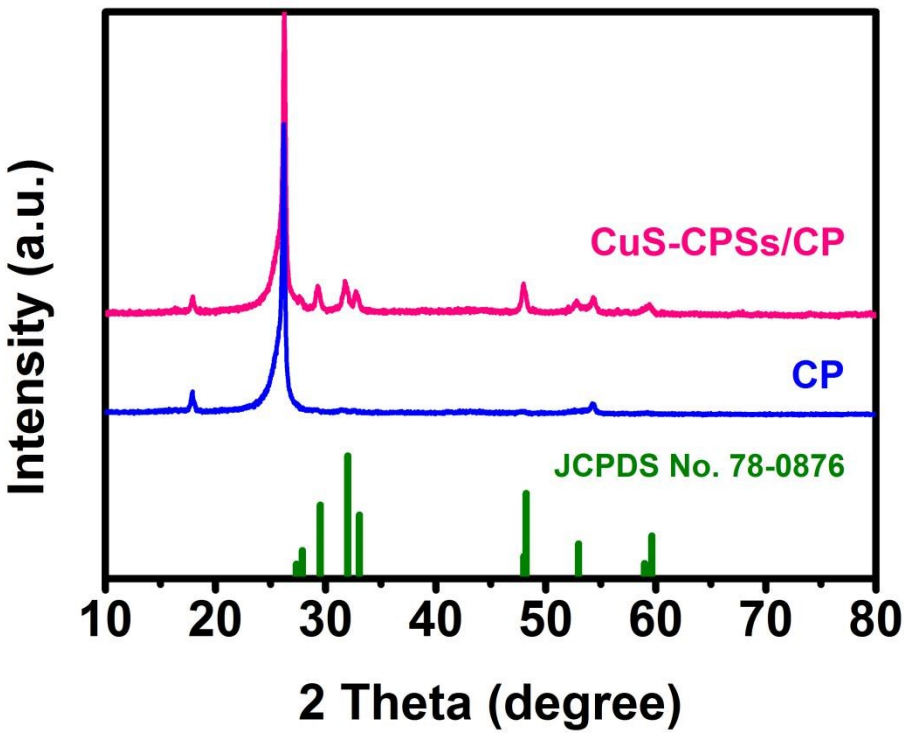

Fig. S19. XRD patterns of CP and post-NRR CuS-CPSs/CP.

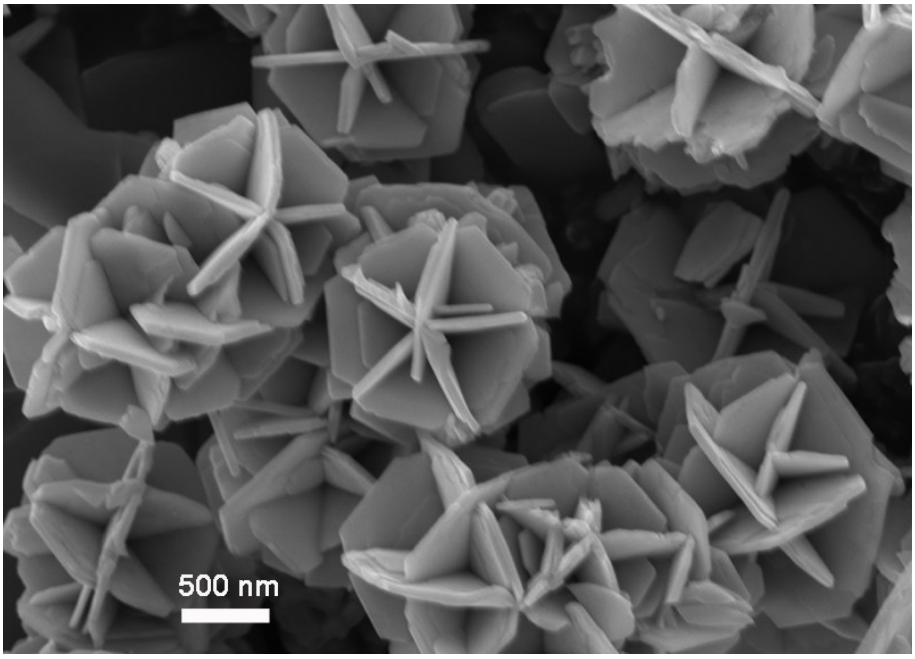

Fig. S20. SEM image of post-NRR CuS-CPSs/CP.

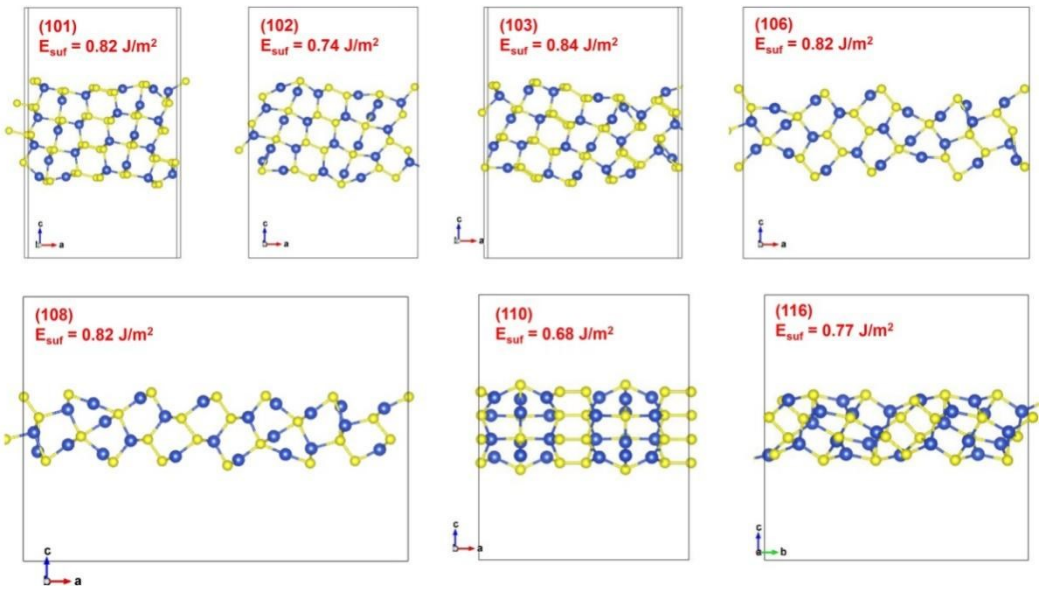

Fig. S21. Surface energies of different facets for CuS.

Table S1. Comparison of electrocatalytic N_2 reduction performance of CuS-CPSs with other NRR electrocatalysts in acidic electrolytes at ambient conditions.

Catalyst	Electrolyte	NH_3 yield	FE (%)	Ref.
CuS-CPSs	0.1 M HCl	18.18 μg h^{-1} $mg^{-1}_{cat.}$	5.63	This work
CoS_2@NC	0.1 M HCl	17.45 μg h^{-1} $mg^{-1}_{cat.}$	4.6	13
FeMoS	0.1 M HCl	8.45 μg h^{-1} $mg^{-1}_{cat.}$	2.96	14
Co-dopd MoS_{2-x}	0.01 M H_2SO_4	0.6 μg h^{-1} $mg^{-1}_{cat.}$	10	15
MoS_2/C_3N_4	0.1 M HCl	18.5 μg h^{-1} $mg^{-1}_{cat.}$	17.8	16
ZrS_2 NF-Vs	0.1 M HCl	30.72 μg h^{-1} $mg^{-1}_{cat.}$	10.33	17
W_2N_3	0.1 M HCl	11.66 μg h^{-1} $mg^{-1}_{cat.}$	11.67	18
MoO_2-OVs	0.1 M HCl	12.2 μg h^{-1} $mg^{-1}_{cat.}$	8.2	19
NPC	0.1 M HCl	0.97 μg h^{-1} $mg^{-1}_{cat.}$	4.2	20
ZrO_2	0.1 M HCl	24.74 μg h^{-1} $mg^{-1}_{cat.}$	5.0	21
Ru single-atoms/Zn	0.1 M HCl	3.665 μg h^{-1} $mg^{-1}_{cat.}$	21	22
$La_2Ti_2O_7$ nanosheet	0.1 M HCl	25.15 μg h^{-1} $mg^{-1}_{cat.}$	4.55	23
Mo nanofilm	0.01 M H_2SO_4	1.89 μg h^{-1} $mg^{-1}_{cat.}$	0.72	24
B-doped graphene	0.05 M H_2SO_4	9.8 μg h^{-1} $mg^{-1}_{cat.}$	10.8	25
N-doped porous carbon	0.05 M H_2SO_4	15.7 μg h^{-1} $mg^{-1}_{cat.}$	1.45	26
$LiMn_2O_4$ nanofiber	0.1 M HCl	15.83 μg h^{-1} $mg^{-1}_{cat.}$	7.44	27
TiC/C nanofiber	0.1 M HCl	14.1 μg h^{-1} $mg^{-1}_{cat.}$	5.8	28
Ag nanosheets	0.1 M HCl	2.83 μg h^{-1} $mg^{-1}_{cat.}$	4.8	29
α-Au/CeO_x-RGO	0.1 M HCl	8.3 μg h^{-1} $mg^{-1}_{cat.}$	10.10	30
Bi nanosheet array	0.1 M HCl	5.26 μg h^{-1} $mg^{-1}_{cat.}$	10.26	31
MoO_3 nanosheets	0.1 M HCl	29.43 μg h^{-1} $mg^{-1}_{cat.}$	1.9	32
Black Phosphorus	0.1 M HCl	31.37 μg h^{-1} $mg^{-1}_{cat.}$	5.07	33

References

1 W. He, H. Jia, X. Li, Y. Lei, J. Li, H. Zhao, L. Mi, L. Zhang and Zhi Zheng, Understanding the formation of CuS concave superstructures with peroxidase-like activity. *Nanoscale*, 2012, **4**, 3501–3506.

2 D. Zhu, L. Zhang, R. E. Ruther and R. J. Hamers, Photo-illuminated diamond as a solid-state source of solvated electrons in water for nitrogen reduction. *Nat. Mater.*, 2013, **12**, 836–841.

3 G. W. Watt and J. D. Chrisp, A spectrophotometric method for the determination of hydrazine. *Anal. Chem.*, 1952, **24**, 2006–2008.

4 A. P. Carvalho, L. A. Meireles and F. X. Malcata, Rapid spectrophotometric determination of nitrates and nitrites in marine aqueous culture media. *Analysis*, 1998, **26**, 347–351.

5 G. Kresse and J. Furthmuller, Efficiency of ab-initio total energy calculations for metals and semiconductors using a plane-wave basis set. *Comp. Mater. Sci.*, 1996, **6**, 15–50.

6 G. Kresse and J. Furthmuller, Efficient iterative schemes for ab initio total-energy calculations using a plane-wave basis set. *Phys. Rev. B*, 1996, **54**, 11169–11186.

7 G. Kresse and J. Hafner, Ab initio molecular-dynamics simulation of the liquid-metal–amorphous-semiconductor transition in germanium. *Phys. Rev. B*, 1994, **49**, 14251–14269.

8 J. Perdew, J. A. Chevary, S. H. Vosko, K. Jackson, M. Pederson, D. J. Singh and C. Fiolhais, Atoms, molecules, solids, and surfaces: Applications of the generalized gradient approximation for exchange and correlation. *Phys. Rev. B*, 1992, **46**, 6671–6687.

9 P. E. Blochl, Projector augmented-wave method. *Phys. Rev. B*, 1994, **50**, 17953–17979.

10 H. J. Monkhorst and J. D. Pack, Special points for brillouin-zone integrations. *Phys. Rev. B*, 1976, **13**, 5188–5192.

11 E. Skulason, T. Bligaard, S. Gudmundsdottir, F. Studt, J. Rossmeisl, F. Abild-Pedersen, T. Vegge, H. Jonsson and J. K. Norskov, A theoretical evaluation of possible transition metal electro-catalysts for N_2 reduction. *Phys. Chem. Chem. Phys.*, 2012, **14**, 1235–1245.

12 H. T. D. Nguyen, Y. B. N. Tran, H. N. Nguyen, T. C. Nguyen, F. Gándara and P. T. K. Nguyen, A series of metal-organic frameworks for selective CO_2 capture and catalytic oxidative carboxylation of olefins. *Inorg. Chem.*, 2018, **57**, 13772–13782.

13 P. Wei, H. Xie, X. Zhu, R. Zhao, L. Ji, X. Tong, Y. Luo, G. Cui, Z. Wang and X. Sun, CoS_2 nanoparticles-embedded N-doped carbon nanobox derived from ZIF-67 for electrocatalytic N_2-to-NH_3 fixation under ambient conditions. *ACS Sustainable Chem. Eng.*, 2020, **8**, 29–33.

14 Y. Guo, Z. Yao, B. J. J. Timmera, X. Sheng, L. Fan, Y. Li, F. Zhang and L. Sun, Boosting nitrogen reduction reaction by bio-inspired FeMoS containing hybrid electrocatalyst over a wide pH range. *Nano Energy*, 2019, **62**, 282–288.

15 J. Zhang, X. Tian, M. Liu, H. Guo, J. Zhou, Q. Fang, Z. Liu, Q. Wu and J. Lou, Cobalt-modulated molybdenum-dinitrogen interaction in MoS_2 for catalyzing ammonia synthesis. *J. Am. Chem. Soc.*, 2019, **141**, 19269–19275.

16 K. Chu, Y. Liu, Y. Li, Y. Guo and Y. Tian, Two-dimensional (2D)/2D interface engineering of a MoS_2/C_3N_4 heterostructure for promoted electrocatalytic nitrogen fixation. *ACS Appl. Mater. Interfaces*, 2020, **12**, 7081–7090.

17 T. Xu, D. Ma, T. Li, L. Yue, Y. Luo, S. Lu, X. Shi, A. M. Asiri, C. Yang and X. Sun, Enhanced electrocatalytic N_2-to-NH_3 fixation by ZrS_2 nanofibers with a sulfur vacancy. *Chem. Commun.*, 2020, **56**, 14031–14034.

18 H. Jin, L. Li, X. Liu, C. Tang, W. Xu, S. Chen, L. Song, Y. Zheng and S. Qiao, Nitrogen vacancies on 2D layered W_2N_3: A stable and efficient active site for nitrogen reduction reaction. *Adv. Mater.*, 2019, **31**, 1902709.

19 G. Zhang, Q. Jia, K. Zhang, Y. Chen, Z. Lie, H. Liu, J. Li and J. Qua, Triggering surface oxygen vacancies on atomic layered molybdenum dioxide for a low energy consumption path toward nitrogen fixation. *Nano Energy*, 2019, **59**, 10–16.

20 P. Song, H. Wang, L. Kang, B. Ran, H. Song and R. Wang, Electrochemical nitrogen reduction to ammonia at ambient conditions on nitrogen and phosphorus co-doped porous carbon. *Chem. Commun.*, 2019, **55**, 687–690.

21 T. Xu, D. Ma, C. Li, Q. Liu, S. Lu, A. M. Asiri, C. Yang and X. Sun, Ambient electrochemical NH_3 synthesis from N_2 and water enabled by ZrO_2 nanoparticles. *Chem. Commun.*, 2020, **56**, 3673–3676.

22 H. Tao, C. Choi, L. Ding, Z. Jiang, Z. Han, M. Jia, Q. Fan, Y. Gao, H. Wang, A. W. Robertson, S. Hong, Y. Jung, S. Liu and Z. Sun, Nitrogen fixation by Ru single-atom electrocatalytic reduction. *Chem*, 2019, **5**, 204–214.

23 J. Yu, C. Li, B. Li, X. Zhu, R. Zhang, L. Ji, D. Tang, A. M. Asiri, X. Sun, Q. Li, S. Liu and Y. Luo, A perovskite $La_2Ti_2O_7$ nanosheet as an efficient electrocatalyst for artificial N_2 fixation to NH_3 in acidic media. *Chem. Commun.*, 2019, **55**, 6401–6404.

24 D. Yang, T. Chen and Z. Wang, Electrochemical reduction of aqueous nitrogen (N_2) at a low overpotential on (110)-oriented Mo nanofilm. *J. Mater. Chem. A*, 2017, **5**, 18967–18971.

25 X. Yu, P. Han, Z. Wei, L. Huang, Z. Gu, S. Peng, J. Ma and G. Zheng, Boron-doped graphene for electrocatalytic N_2 reduction. *Joule*, 2018, **2**, 1610–1622.

26 X. Yang, K. Li, D. Cheng, W. Pang, J. Lv, X. Chen, H. Zang, X. Wu, H. Tan, Y. Wang and Y. Li, Nitrogen-doped porous carbon: Highly efficient trifunctional electrocatalyst for oxygen reversible catalysis and nitrogen reduction reaction. *J. Mater. Chem. A*, 2018, **6**, 7762–7769.

27 C. Li, J. Yu, L. Yang, J. Zhao, W. Kong, T. Wang, A. M. Asiri, Q. Li and X. Sun, An efficient electrocatalyst for N_2 reduction to NH_3 under ambient conditions. *Inorg. Chem.*, 2019, **58**, 9597–9601.

28 G. Yu, H. Guo, W. Kong, T. Wang, Y. Luo, X. Shi, A. M. Asiri, T. Li and X. Sun, Electrospun TiC/C nanofibers for ambient electrocatalytic N_2 reduction. *J. Mater. Chem. A*, 2019, **7**, 19657–19661.

29 H. Huang, L. Xia, X. Shi, A. M. Asiri and X. Sun, Ag nanosheets for efficient electrocatalytic N_2 fixation to NH_3 under ambient conditions. *Chem. Commun.*, 2018, **54**, 11427–11430.

30 S. Li, D. Bao, M. Shi, B. Wulan, J. Yan and Q. Jiang, Amorphizing of Au nanoparticles by CeOx-RGO hybrid support towards highly efficient electrocatalyst for N_2 reduction under ambient conditions. *Adv. Mater.*, 2017, **29**, 1700001.

31 R. Zhang, L. Ji, W. Kong, H. Wang, R. Zhao, H. Chen, T. Li, B. Li, Y. Luo and X. Sun, Electrocatalytic N_2-to-NH_3 conversion with high faradaic efficiency enabled using a Bi nanosheet array. *Chem. Commun.*, 2019, **55**, 5263–5266.

32 J. Han, X. Ji, X. Ren, G. Cui, L. Li, F. Xie, H. Wang, B. Li and X. Sun, MoO_3 nanosheets for efficient electrocatalytic N_2 fixation to NH_3. *J. Mater. Chem. A*, 2018, **6**, 12974–12977.

33 L. Zhang, L. Ding, G. Chen and X. Yang and H. Wang, Ammonia synthesis under ambient conditions: Selective electroreduction of dinitrogen to ammonia on black phosphorus nanosheets. *Angew. Chem. Int. Ed.*, 2019, **58**, 2612–2616.